Bioorganic Chemistry 104 (2020) 104208

Contents lists available at ScienceDirect

Bioorganic Chemistry

journal homepage: www.elsevier.com/locate/bioorg

Design, synthesis and biological evaluation of novel plumbagin derivatives as potent antitumor agents with STAT3 inhibition

Na Li, Jinfeng Ou, Na Bao, Cheng Chen, Zhixian Shi, Li Chen*, Jianbo Sun**

State Key Laboratory of Natural Medicines, Department of Natural Medicinal Chemistry, School of Traditional Chinese Pharmacy, China Pharmaceutical University, 24 Tong Jia Xiang, Nanjing 210009, People's Republic of China

ARTICLE INFO

Keywords:
Plumbagin
Antiproliferation
STAT3 inhibition
Apoptosis
Antitumor

ABSTRACT

Based on the structure of signal transducer and activator of transcription 3 (STAT3), a series of 1,4-naphthoquinones derived from plumbagin (PL) with STAT3 inhibition potential were designed, synthesized, and biologically evaluated *in vitro* against several human cancer cell lines (MDA-MB-231, HepG2 and A549 cells) and three normal cells. The structure–activity relationship (SAR) and molecular docking result showed that the presence of hydroxyl group at C-5 of PL might interact with STAT3 in the form of hydrogen bonds, which is conducive to the binding of this kind structures with STAT3. Among the target compounds, **7a** displayed the most potent inhibition against cancer cells and weaker cytotoxicity on normal cells than PL. The western bolting analysis showed that **7a** could suppress the phosphorylation of STAT3 as well as the downstream genes instead of affecting its upstream tyrosine kinases (Src and JAK2) levels and p-STAT1 expression. Furthermore, molecular docking indicated that **7a** bound to STAT3 more tightly than PL, and it could significantly induce the apoptosis of cancer cells *in vitro*. All these results may provide reference for the discovery of effective STAT3 inhibitors.

1. Introduction

Signal transducer and activator of transcription 3 (STAT3) is a member of the STAT family of transcription factors. Activated STAT3 can mediates the signal transduction which is closely related to cell proliferations, differentiations and apoptosis [1–2]. Generally, the activation of STAT3 is under careful control to ensure the proliferation of normal cells. However, it is found that STAT3 is activated aberrantly in several cancer types, such as breast, lung, prostate, ovarian [3–6]. Furthermore, introduction of antisense, dominant negative, and decoy oligonucleotides against STAT3 lead to significant apoptosis of cancer cells [7]. Therefore, inhibition of STAT3 activity has long been an attractive strategy in cancer therapy [8–9].

The STAT3 activation needs several procedures. Generally, cytokines or growth factors or platelet-derived growth factor (PDGF) mediate the phosphorylation of STAT3 via its Src homology 2 (SH2) domain [10–11]. The phosphorylated STAT3 (p-STAT3) dimerizes through the same domain and then translocate to the nucleus, where it initiates transcription of its target genes [12–13]. These findings support the hypothesis that phosphorylation of STAT3 on SH2 domain is a key event in the STAT3 activation, which provides an attractive strategy in the discovery of STAT3 inhibitor [14–15]. Currently, many inhibitors targeting STAT3-SH2 have been reported, such as S3l-20 l, STA-21 and Stattic. However, none of them have been approved clinically due to their defects on permeability, stability and/or side effect [16–22]. Therefore, discovery of novel STAT3-SH2 inhibitors is essential for the elucidation of the structure–activity relationship and the development of STAT3-SH2 inhibitors as precision anticancer agents.

Plumbagin (PL) is a natural 1,4-naphthoquinone isolated from the plant *Plumbago zeylanica* [23]. 1,4-naphthoquinone1 is an important class of small molecules for the the design of anticancer agents [24–25]. Previous studies reported that PL showed potential anticancer activity against breast cancer, which was mainly due to the inhibition of STAT3 phosphorylation [26]. Moreover, PL shares a very similar structure with STA-21 and LLL-3 which were efficient STAT3-SH2 inhibitors (Fig. 1A). Therefore, it is very promising to optimize the structure of PL to development novel STAT3 inhibitors based on the protein crystal structure of STAT3 and its pharmacophore model.

2. Results and discussion

2.1. Design

The pTyr705 site and the side pocket (Fig. 1B) in STAT3-SH2

* Corresponding author.
** Corresponding author.
E-mail addresses: chenli627@cpu.edu.cn (L. Chen), sjbcpu@gmail.com (J. Sun).

https://doi.org/10.1016/j.bioorg.2020.104208
Received 4 May 2020; Received in revised form 15 August 2020; Accepted 25 August 2020
Available online 28 August 2020

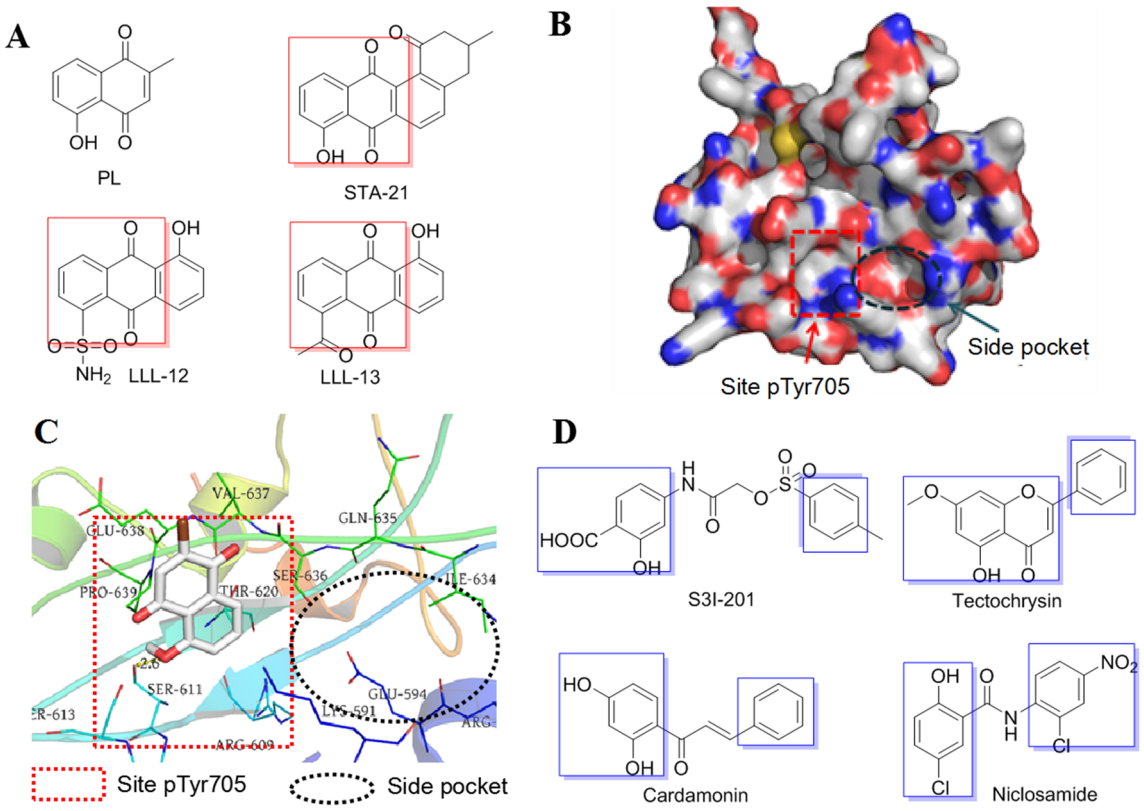

Fig. 1. The analysis of various small-molecule STAT3 inhibitors (STAT3-SH2 site). (A) The structures of several STAT3 inhibitors. (B) Two main binding sites of STAT3-SH2 (PDB ID: 1BG1). (C) The binding mode of PL with STAT3-SH2 domain (1BG1). (D) The structures of several STAT3 inhibitors.

domain were two hot binding sites of small molecule STAT3 inhibitors. STAT3 protein ligands that can bind to the STAT3-SH2 domain generally contain three classic structural features: two aromatic rings (occupying the Site pTyr705 and Side pocket regions, respectively) and the bridge chain that connects them. To increase the binding affinity of planner scaffold (PL), we were promoted to introduce an aromatic ring to occupy the side pocket. And the most suitable linker should allow sufficient flexibility for PL and another aromatic ring to bind pTyr705 site and side pocket, respectively. According to the reported structure of the potent small molecule STAT3 inhibitors, it was found that the linkers could accommodate 0–5 sp^3 or sp^2 atoms and exist to be amide in most cases. Therefore, seven linkers including amino or amide (P1-P7) were chosen to form different compounds and were quickly screened via computational docking for the final design. The binding mode of PL and STAT3-SH2 domain were predicted using software Autodock Vina 1.1.2 [27]. As shown in Fig. 1C, PL could embed in pTyr705 pocket by forming a hydrogen bond with residue Ser611 and cation-π interaction with residue Lys591, but it could not interact with the side pocket. Various STAT3-SH2 inhibitors (such as STA-21, S3I-201 and cardamonin, Fig. 1D) usually contain benzene, naphthoquinone or quinoline to bind STAT3-SH2 domain. Based on the above analysis, the introduction of an aromatic ring in PL may allow the new derivatives to bind the two pockets simultaneously, thereby increasing the STAT3 binding affinity of PL.

Then, PL was connected to an aromatic ring via seven linkers (Fig. 2A), which were docked to the STAT3 SH2 domain (PDB entry 1BG1). As shown in Fig. 2B, P4 showed a higher STAT3-SH2 affinity than the others. Thus, the linker in P4 was selected to introduce the aromatic ring to PL. In addition, in order to investigate the effects of the hydroxyl group (C-5) on the anti-proliferative activity of PL, menodione was also selected as a parent compound to synthesize several new derivatives (Fig. 3).

2.2. Chemistry

The synthetic routes of target compounds (**7a-9b**) were shown in Scheme 1. In brief, the syntheses began with the condensation between β-alanine and differently substituted benzoyl chloride (**1a-g**) in the presence of NaOH, which quickly yielded intermediates **2a-g**. Additionally, **5** was yielded by debenzylation of **3** and nicotinoyl chloride (**4**). The intermediate **6** was obtained from **5** in the presence of Pd/C and H_2. Compounds **7a-9b** were obtained by Kochi-Anderson reaction of PL or menadione using different intermediates [28]. In addition, the yields of Kochi-Anderson reaction were low (products and a lot of reactant) in this study, which were due to the mild reaction conditions.

In order to further analyze the structure–activity relationship (SAR) of these derivatives, compounds **11–13** were prepared (Scheme 2). Kochi-Anderson reaction between PL and succinic acid yielded **10** which was then condensed with aniline in the presence of benzotriazol-1-yl-oxytripyrrolidinophosphonium hexafluorophosphate (PyBop) and 4-dimethylaminopyridine (DMAP) to produce **11**. The oxidative addition reaction of PL with aniline catalyzed by $Cu(AcO)_2$ yielded **12**. Compound **13** was obtained from the ammonolysis of PL.

2.3. In vitro anti-proliferative activity

The inhibition rates of all the derivatives and their parent compounds (PL and menadione) were first evaluated against MDA-MB-231 by MTT assay (Table 1). The results showed that the PL derivatives generally displayed a higher antiproliferative activity than the menadione derivatives. For example, **7a-7d/9a** (derived from PL) showed higher activity (65.18–96.63%) than **8a-8g/9b** (derived from menadione, 16.76–46.38%), which suggesting that the hydroxyl groups at C-5 were essential for the activities of these compounds. Furthermore, **11–13** showed much lower activity (31.87%-48.34%) than **7a** (91.86%), which indicated that the linker in **7a** was suitable for the

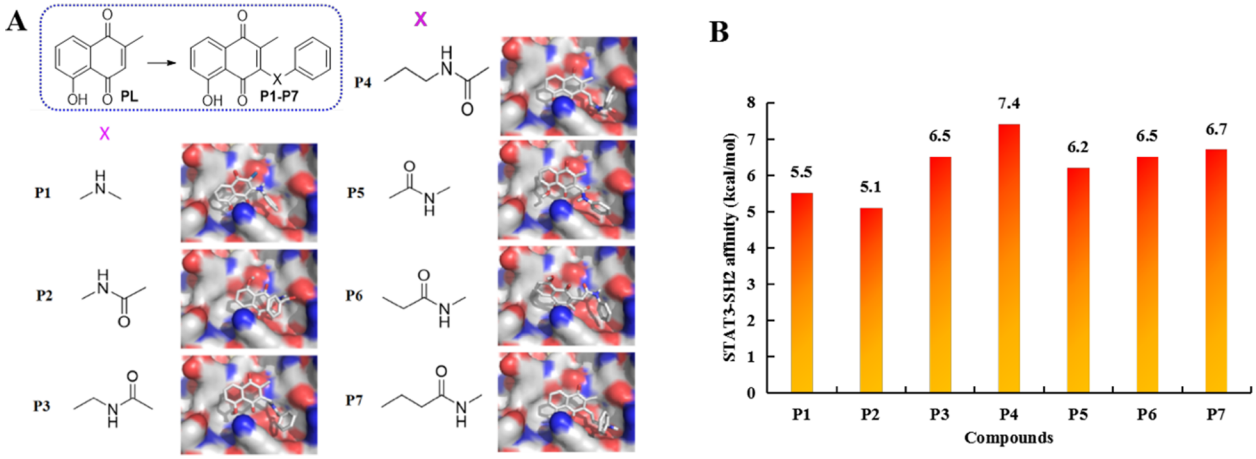

Fig. 2. Analysis of molecular docking of P1-P7. (A) Docking mode of P1-P7 with STAT3 (PDB ID). (B) Docking Scores of P1-P7.

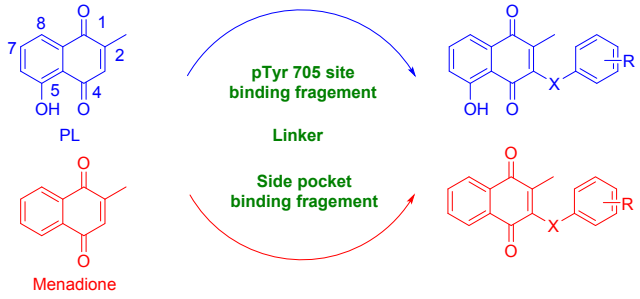

Fig. 3. Design strategy of the new STAT3 inhibitors derived from PL and menadione.

promotion of the activity (Fig. 4A). In addition, we found that the groups in benzene ring could affect the activity. As shown in Fig. 4B, although electron-withdrawing groups substituted on benzene were generally benefit for the inhibition (**7b** *vs.* **7e**/**7g**), the compound (**7a**) which introduced benzene exhibited the most potential.

Next, **7a-7d** and **9a** with enhanced inhibitory activity than PL were selected to determine their IC_{50} values against three cancer cell lines (MDA-MB-231, HepG2 and A549). As shown in Table 2, compared to PL (IC_{50}: 10.66–14.23 μM), increased activities were found in **7a**, **7b** and **9a** (IC_{50}: 6.01–8.75 μM), which were selected for further investigation of cytotoxicity against three normal human cell lines (MDA-MB-10A, PBMCs and HFL-1 cells). It is worth mentioned that **7a** showed a lower cytotoxicity than **7b, 9a** and PL. Combined with the high selective index (SI) of **7a** in breast cancer cells, **7a** was preferentially selected for further investigation in MDA-MB-231.

2.4. Compound *7a* inhibited the phosphorylation of STAT3 at site pTyr705

To further investigate whether the effects of **7a** was related to phosphorylation of STAT3, the level of p-STAT3 stimulated by IL-6 in MDA-MB-231 was evaluated. As displayed in Fig. 5, **7a** could effectively decrease the level of p-STAT3 at site pTyr705 in a concentration-

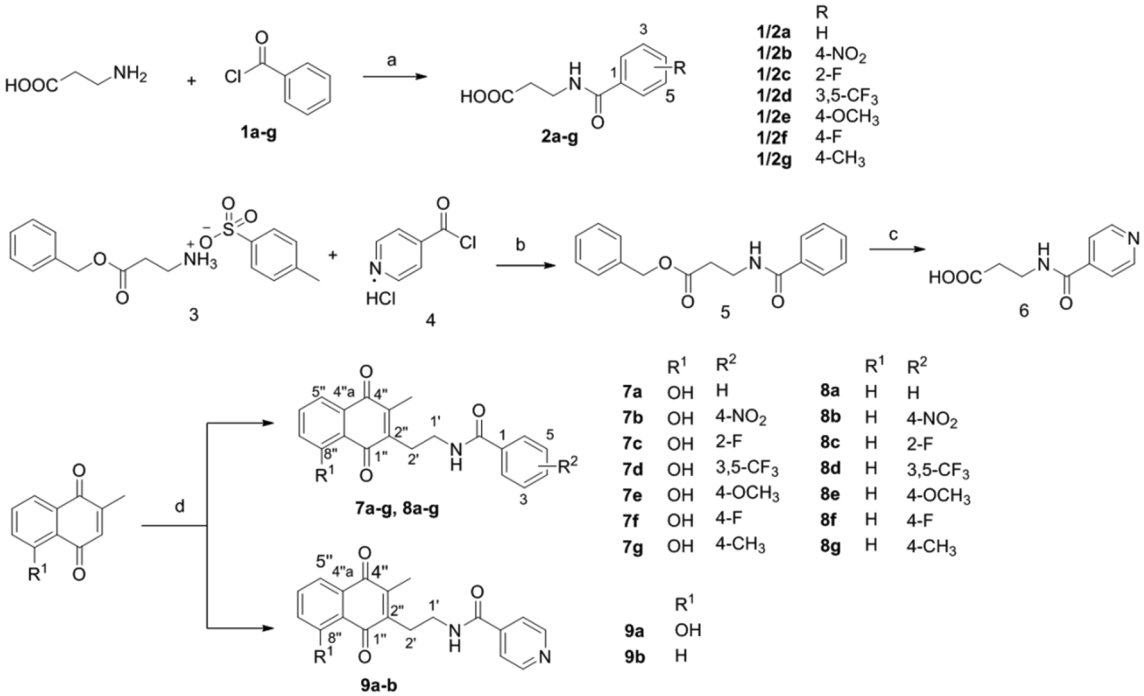

Scheme 1. Reagents and conditions: (a) 10% NaOH, rt, 30 min. (b) DIPEA, dry DCM, 0 °C to r.t., 6 h. (c) H_2, Pd/C. (d) **2a-g** or **6** (3.0 eq), silver nitrate (0.3 eq), ammonium persulfate (1.3 eq), aq·H_2O/CH_3CN (V/V = 3:4), 100 °C, 3–6 h.

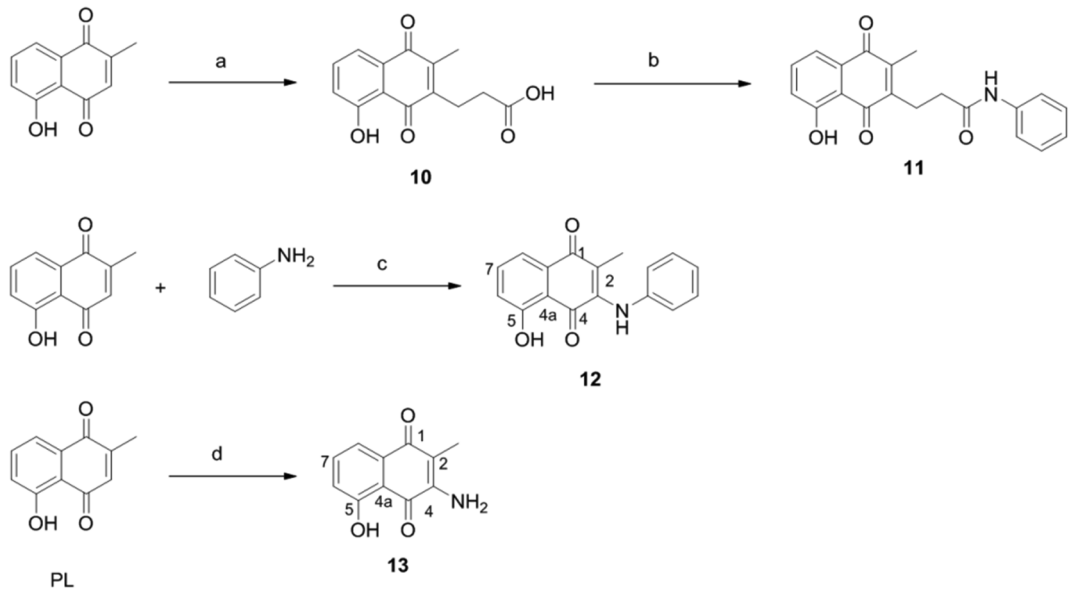

Scheme 2. Reagents and conditions: (a) succinic acid, $AgNO_3$, $(NH_4)_2S_2O_8$, 30% CH_3CN, 65–70 °C, 3 h, (b) aniline, PyBop, DMAP, TEA, rt, 12 h. (c) $Cu(AcO)_2$, AcOH, 60 °C, 4 h. (d) MeOH, NaN_3, N_2, NH_3, 50 °C, 5 h.

dependent manner and the function of **7a** was stronger than that of PL. However, the level of total STAT3 was not changed with the treatment of **7a**. These results indicated that **7a** could inhibit the phosphorylation of STAT3 at site pTyr705.

2.5. Compound *7a* inhibited the expression of the downstream gene of STAT3

According to what has been mentioned above, compound **7a** could inhibit the level of STAT3. To further study the effects of **7a** on the STAT3 pathway, we examined the expressions of STAT3-targeted genes (Survivin and Mcl-1). As shown in Fig. 6, compound **7a** down-regulated the level of STAT3 downstream genes. These results preliminarily indicated that **7a** could inhibit the activity of STAT3.

2.6. Compound *7a* had no effects on the typical upstream kinases of STAT3

The phosphorylation of STAT3 also can be mediated by STAT3 upstream tyrosine kinases, such as p-JAK2 and p-Src. To evaluate whether the p-STAT3 inhibition of **7a** brought about the regulation of Src and JAK2, western blot was carried out. It was obvious in Fig. 7 that the levels of p-Src and p-JAK2 as well as total proteins were not influenced by **7a**, which illustrating that **7a** might inhibit the phosphorylation of STAT3 by binding to STAT3 protein.

2.7. Compound *7a* had no effects on the phosphorylation of STAT1

As a STAT isoform, inhibition of STAT1 phosphorylation can promote the survival of tumors, which is opposite to the function of STAT3 [29]. Then, we detected whether **7a** displayed an inhibition to p-STAT1. As shown in Fig. 8, the level of p-STAT1 was slightly changed with the treatment of **7a**. This result indicated that **7a** might show a much higher inhibition on p-STAT3 than p-STAT1 in terms of suppressing the survival of cancer cells.

Combined with the expression of STAT3 and STAT1, it showed that **7a** displayed the most effective concentration dependent inhibition of STAT3, but has no effect on the expression of STAT1. This result indicated that **7a** might inhibited the survival of cancer cells through the combination of STAT3, and did not show the characteristics of pan active structures.

2.8. Molecular docking of *7a* to the STAT3 protein

As mentioned above, **7a** might bind to STAT3. To further speculate the binding sites of **7a**, molecular docking was adopted. **7a** could embed into the key pockets related to the phosphorylation of STAT3 (Fig. 9). One hydrogen bond (between hydroxyl group and Arg609) and two cation-π interactions (between the aromatic ring and Lys591; between the benzene and Arg595) might support **7a** binding to the SH2 domain more tightly, thereby inhibiting the phosphorylation of STAT3. Therefore, introduction of a suitable substituents at C-5 to from a new interaction with STAT3 could enhance the combination of small molecular with STAT3 hopefully.

Table 1
Preliminary inhibitory effects of the tested compounds at 20 μM on MDA-MB-231 cells.

Comp.	Inhibition rate % [a]	Comp.	Inhibition rate % [a]	Comp.	Inhibition rate % [a]
7a	97.86 ± 6.35	**8a**	16.76 ± 1.51	**9a**	96.63 ± 8.55
7b	93.63 ± 7.69	**8b**	20.54 ± 1.95	**9b**	19.87 ± 1.73
7c	81.48 ± 7.59	**8c**	35.65 ± 2.99	**11**	31.87 ± 1.98
7d	65.18 ± 5.26	**8d**	18.45 ± 1.02	**12**	46.38 ± 3.26
7e	19.76 ± 1.44	**8e**	32.21 ± 2.47	**13**	48.34 ± 2.89
7f	23.13 ± 1.48	**8f**	46.38 ± 3.59	PL	90.56 ± 8.41
7g	18.59 ± 1.25	**8g**	23.54 ± 1.56	menadione	36.33 ± 2.11

[a] MTT methods, cells were incubated with corresponding compounds for 48 h. Values are mean of three independent experiments.

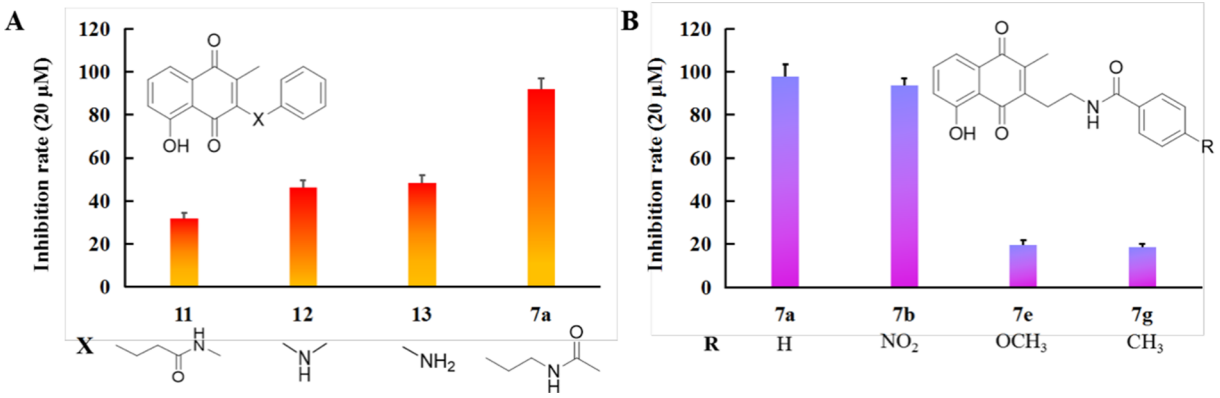

Fig. 4. Comparison of inhibition rates of partial target compounds. (A) Inhibition rates of **11–13** and **7a** at 20 μM in MDA-MB-231 cells. (B) Inhibition rates of **7a**, **7b**, **7e** and **7g** at 20 μM in MDA-MB-231 cells.

Table 2
IC_{50} values of the tested compounds against cancer cells and normal human cells.

Comp.	IC_{50} (μM)[a]						SI[b]
	MDA-MB-231	HepG2	A549	MDA-MB-10A	PBMCs	HFL-1	MDA-MB-10A/MDA-MB-231
7a	6.01 ± 0.22	7.20 ± 0.52	7.02 ± 0.46	26.54 ± 1.29	25.69 ± 1.68	12.52 ± 0.98	4.42
7b	11.19 ± 1.73	10.95 ± 2.40	11.98 ± 1.22	20.14 ± 1.66	23.52 ± 1.57	11.38 ± 1.01	1.80
7c	16.02 ± 2.21	17.08 ± 2.62	8.34 ± 1.45	ND[c]	ND	ND	ND
7d	19.36 ± 0.73	19.56 ± 0.47	12.85 ± 2.02	ND	ND	ND	ND
9a	7.69 ± 0.77	8.75 ± 0.97	7.98 ± 0.35	11.42 ± 0.74	10.24 ± 0.84	14.68 ± 1.23	1.49
PL	14.23 ± 0.93	10.66 ± 1.54	12.40 ± 1.08	9.12 ± 0.49	10.12 ± 0.72	3.21 ± 0.24	0.64

[a] MTT methods, cells were incubated with corresponding compounds for 48 h. IC_{50} (μM) values (means ± SD, n = 3).
[b] Selective index;
[c] Not determined.

2.9. The morphological apoptosis induced by 7a

The inhibition of STAT3 signaling pathway usually causes significant apoptosis in cancer cells. The morphological apoptosis caused by **7a** was then detected by Hoechst 33,342 staining. It was clear that the cells were killed obviously by the treatment of **7a**. Simultaneously, the apoptotic cells were stained with light blue (white arrows, Fig. 10). These results illustrated that **7a** could induce apoptosis of cancer cells.

2.10. Effects of 7a on cell apoptosis

In order to further quantitatively evaluated the apoptosis induced by **7a**, an annexin V-FITC/PI dual staining assay was used in MDA-MB-231 cells. As shown in Fig. 11A, after 48 h of treatment with **7a**, apoptosis was induced in a dose-manner. Furthermore, at a concentration of 15 μM, the apoptotic cells induced by **7a** accounted for 24.4% of the cells, which was much higher than that of parent compound PL (13.3%) (Fig. 11B). These results suggested that the capability of inducing apoptosis of **7a** was enhanced compared to PL.

3. Conclusions

In summary, a series of compounds derived from PL or menadione were designed, synthesized, and biologically evaluated with STAT3 inhibitory activity. SARs revealed that the hydroxyl group (C-5) was important for the activity. According to the above results and the reported inhibitors, we found that the formation of hydrogen bond between suitable substituents at C-5 and STAT3 might enhance the combination of small molecular with STAT3. Thus, the presence of OH at C-5 in PL derivatives could interact with STAT3 in the form of hydrogen bond, which was conducive to the binding of this kind structure to STAT3. In addition, the introduction of additional groups in aromatic

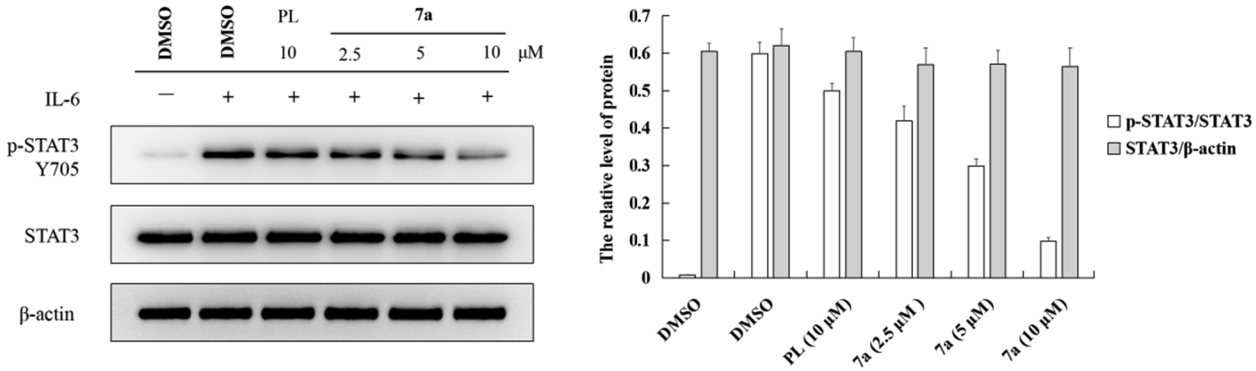

Fig. 5. Compound **7a** inhibited STAT3 phosphorylation in MDA-MB-231. The MDA-MB-231 were serum-starved overnight, then left untreated or treated with PL (10.0 μM) and **7a** (2.5, 5.0, 10 μM) for 6 h, followed by stimulation by IL-6 (25 ng/mL). The cells were harvested at 30 min and analyzed by Western blot assays.

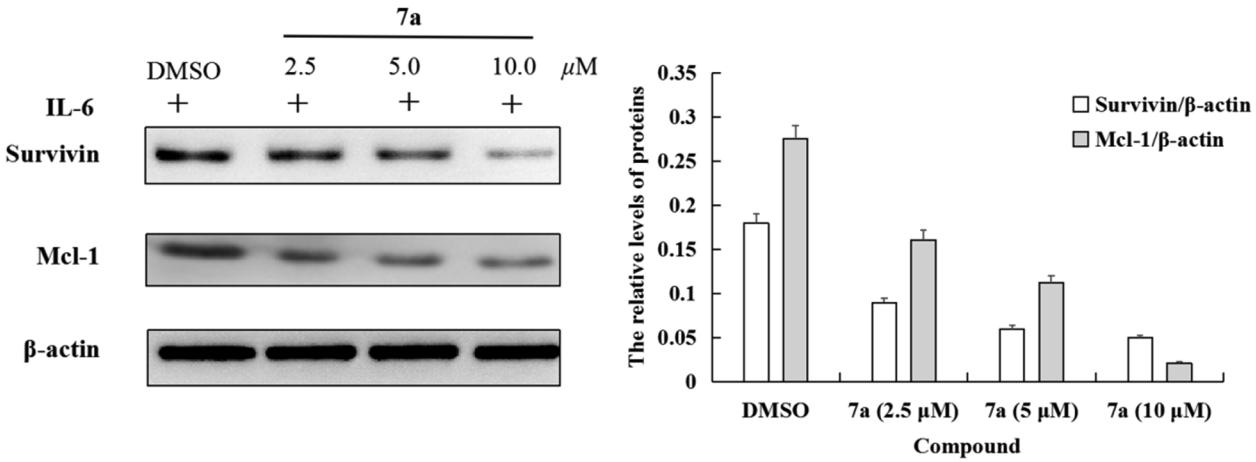

Fig. 6. Effects of compound **7a** on expression of STAT3 downstream genes (Survivin and Mcl-1) in MDA-MB-231. The MDA-MB-231 were serum-starved overnight, then treated with DMSO or **7a** (2.5, 5.0, 10 μM) for 6 h, followed by stimulation by IL-6 (25 ng/mL). The cells were harvested at 30 min and analyzed by Western blot assays.

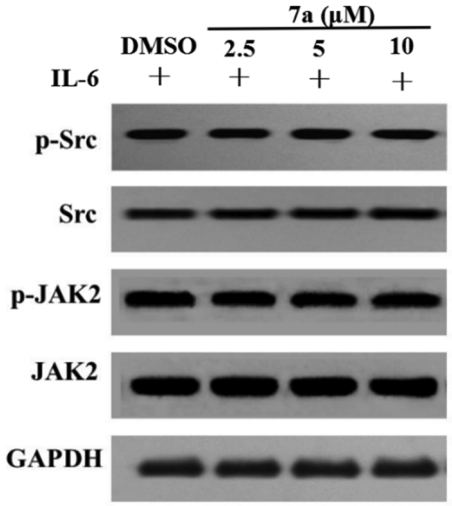

Fig. 7. Effects of compound **7a** on upstream kinases of STAT3 in MDA-MB-231. MDA-MB-231 were serum-starved overnight, then treated with DMSO or **7a** (2.5, 5.0, 10 μM) for 6 h, followed by stimulation by IL-6 (25 ng/mL). The cells were harvested at 30 min and analyzed by Western blot assays.

ring and suitable linkers could also contribute to the activity. These preliminary results might provide a theoretical basis for the further development of STAT3 inhibitors. Among the target compounds, **7a** displayed the most potent inhibition. Western blotting showed that **7a** could inhibit the phosphorylation of STAT3 as well as the downstream genes without affecting the activated Src, JAK2 and STAT1. Furthermore, the docking studies revealed that compound **7a** could bind to the SH2 domain of STAT3 protein more tight than PL. This function allowed **7a** induced a superior apoptosis against cancer cells compared to PL. Together, these results warranted its potential to be a promising STAT3 inhibitor in the cancer treatment.

4. Experimental

4.1. Chemistry

All reagents were purchased from commercial companies. ^{1}H NMR and ^{13}C NMR spectra were recorded on a Bruker AVANCE instrument at 25 °C. The molecular weights were detected on HP 1100LC/MSD spectrometer.

4.1.1. Syntheses of intermediates and final compounds

*4.1.1.1. General procedures for the preparation of **2a-2g**.* Corresponding acyl chloride (**1a-1g**, 5 mmol) was added to a solution of β-alanine (489.5 mg, 5.5 mmol) in sodium hydroxide solution (5 M, 2 mL). Sodium hydroxide solution (5 M) was added to the mixture to keep the pH was 9–10. After 30 min, the reaction was washed with CH_2Cl_2 (5 mL) and the water layer was poured into 20 mL of ice water, the pH of mixture was changed to 2 with HCl (1 M), filtered, then washed with excess cold water and dried. The intermediates were obtained as white solids.

*4.1.1.2. Syntheses of **6**.* DIPEA (645 mg, 5 mmol) was added to a

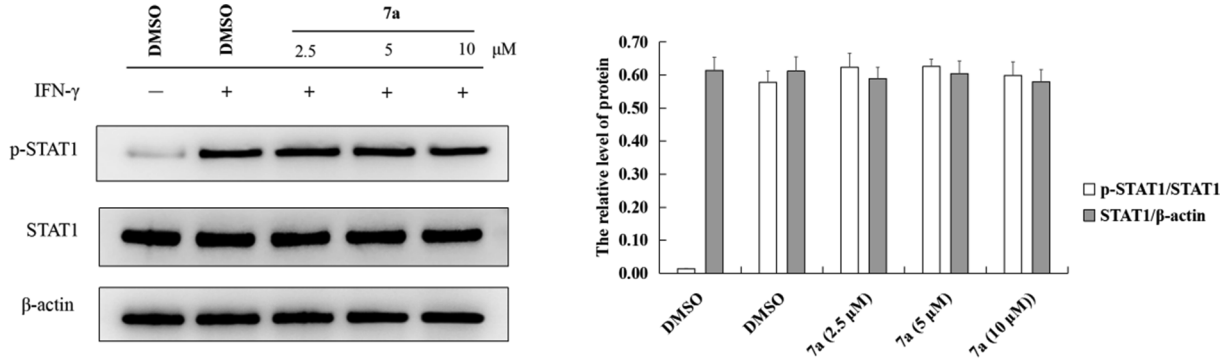

Fig. 8. Effects of compound **7a** on STAT1 phosphorylation in MDA-MB-231. MDA-MB-231 were serum-starved overnight, then treated with DMSO or **7a** (2.5, 5.0, 10 μM) for 6 h, followed by stimulation by IFN-γ (50 ng/mL). The cells were harvested at 30 min and analyzed by Western blot assays.

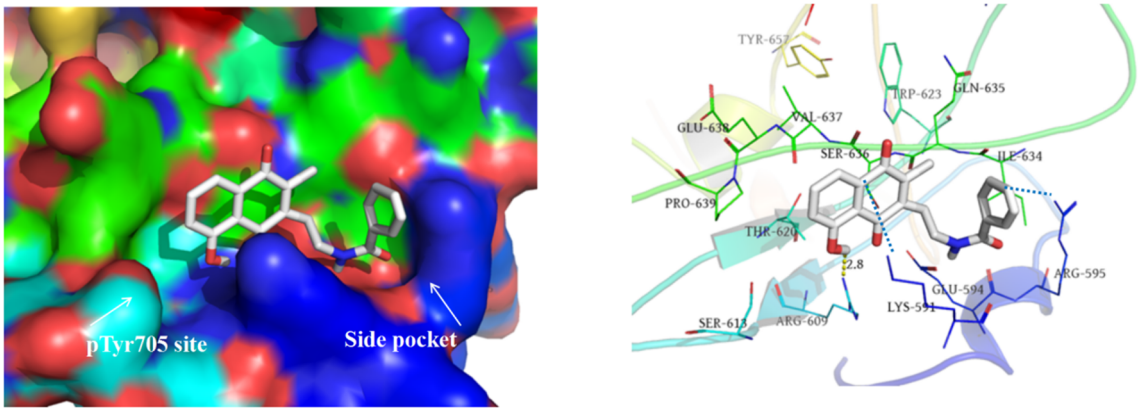

Fig. 9. Docking model of **7a** with the STAT3 SH2 domain. The protein (PDB ID 1BG1) was shown in a cartoon representation. Hydrogen bonds were shown as dashed yellow lines and cation-π interactions shown as blue dashed lines. (For interpretation of the references to colour in this figure legend, the reader is referred to the web version of this article.)

solution of **3** (737 mg, 2.1 mmol) in dry CH_2Cl_2 (5 mL) at 0 °C. Nicotinyl chloride (**4**, 356 mg, 2 mmol) was added slowly to the mixture after 10 min and stirred for 6 h at r.t. Then the reaction solution was added into CH_2Cl_2 (15 mL), washed by sodium hydroxide solution (0.5 M, 3 × 15 mL). The organic layer was dried with Na_2SO_4 and the solvent was evaporated. The crude material was purified via column chromatography (PE/EA = 1:3) to yield **5** (159 mg, 56%). Pd/C (100 mg) was added to a solution of **5** (1.8 mmol) in MeOH (15 mL). The mixture was sonicated at 50 °C under H_2 for 12 h and then filtered with tripoli and the filtrate evaporated. The crude material was purified via column chromatography (PE/EA = 1:3) to yield **6** (252 mg, 71%).

*4.1.1.3. General procedures for the preparation of **7a-8g**.* Corresponding intermediates (3 mmol, 3.0 eq), $AgNO_3$ (47.3 mg, 0.28 mmol, 0.28 eq) were successively added to a solution of PL (188 mg, 1 mmol, 1.0 eq) or menadione (172 mg, 1 mmol, 1.0 eq) in aqueous acetonitrile (CH_3CN/H_2O = 4:3, 18 mL) at 60 °C. Then the reaction was heated to 70 °C. Next, a solution of ammonium persulfate (0.8 mmol, 1.3 eq, CH_3CN/H_2O = 4:3, 10 mL) was added dropwise over 30 min, and the resulting solution stirred at 65–70 °C for 3–4 h. On cooling, the mixture was extracted with EtOAc (3 × 20 mL), and the organic layer was washed with H_2O (3 × 20 mL), saturated $NaHCO_3$ (4 × 20 mL), dried and solvent evaporated. The crude material was purified via column chromatography (PE/EA = 10:1) to yield **7a-9b**.

*4.1.1.3.1. N-(2′-(8′′-hydroxy-3′′-methyl-1′′,4′′-dioxo-1,4-dihydronaphthalen-2′′-yl)ethyl)benzamide (**7a**).* Yellow oil, 93 mg (28% yield). ^{1}H NMR (300 MHz, $CDCl_3$) δ_H 12.12 (s, 1H), 7.72 (d, J = 8.4 Hz, 2H), 7.61 (m, 2H), 7.48 (m, 3H), 7.23 (dd, J = 7.8 Hz, 1.8 Hz, 1H), 6.57 (s, 1H), 3.65 (q, J = 6.9 Hz, 2H), 3.02 (t, J = 6.6 Hz, 2H), 2.27(s, 3H). ^{13}C NMR (75 MHz, $CDCl_3$) δ_C 189.5, 166.7, 160.3, 145.9, 142.7, 135.2, 130.6, 127.6, 125.8, 125.8, 122.9, 118.2, 38.0, 25.5, 12.1. ESI/HRMS (m/z) $[M+H]^+$ 336.1227. Calcd for $[C_{20}H_{18}NO_4]$: 336.1236.

*4.1.1.3.2. N-(2′-(8′′-hydroxy-3′′-methyl-1′′,4′′-dioxo-1,4-dihydronaphthalen-2′-yl)ethyl)-4-nitrobenzamide (**7b**).* Yellow oil, 114 mg (38% yield). ^{1}H NMR (300 MHz, $CDCl_3$) δ_H 12.05 (s, 1H), 8.29 (d, J = 9.0 Hz, 2H), 7.90 (d, J = 9.0 Hz, 2H), 7.62 (m, 2H), 7.23 (d, J = 1.8 Hz, 1H), 6.70 (s, 1H), 3.68 (t, J = 6.3 Hz, 2H), 3.04 (t, J = 6.6 Hz, 2H), 2.28 (s, 3H). ^{13}C NMR (75 MHz, $CDCl_3$) δ_C 204.6, 161.3, 136.5, 130.9, 128.0, 124.1, 124.0, 119.3, 39.3, 26.2, 13.1. ESI/HRMS (m/z) $[M+H]^+$ 381.1080. Calcd for $[C_{20}H_{17}N_2O_6]$: 381.1087.

*4.1.1.3.3. 2-fluoro-N-(2′-(8′′-hydroxy-3′′-methyl-1′′,4′′-dioxo-1,4-dihydronaphthalen-2′′-yl)ethyl)benzamide (**7c**).* Yellow oil, 127 mg (36% yield). ^{1}H NMR (300 MHz, $CDCl_3$) δ_H 12.15 (s, 1H), 8.07 (td, J = 8.4 Hz, 1.8 Hz, 1H), 7.59 (m, 2H), 7.45 (m, 1H), 7.23 (m, 2H), 7.11 (dd, J = 12.0 Hz, 7.5 Hz, 1H), 7.04 (s, 1H), 3.68 (q, J = 6.0 Hz, 2H), 3.04 (t, J = 6.9 Hz, 2H), 2.27(s, 3H). ^{13}C NMR (75 MHz, $CDCl_3$) δ_C 189.1, 183.1, 162.6, 160.2, 145.7, 142.5, 135.0, 132.4, 132.3, 131.0, 130.9, 123.8, 122.8, 118.0, 115.2, 114.8, 113.8, 38.0, 25.5, 12.0. ESI/HRMS (m/z) $[M+H]^+$ 354.1136. Calcd for $[C_{20}H_{17}FNO_4]$: 354.1142.

*4.1.1.3.4. N-(2′-(8′′-hydroxy-3′′-methyl-1′′,4′′-dioxo-1,4-dihydronaphthalen-2′′-yl)ethyl)-3,5-bis(trifluoromethyl)benzamide (**7d**).* Yellow oil, 131 mg (28% yield). ^{1}H NMR (300 MHz, $CDCl_3$) δ_H 12.00 (s, 1H), 8.49 (d, J = 9.0 Hz, 3H), 8.08 (d, J = 8.7 Hz, 1H), 7.82 (m, 2H), 6.89 (s, 1H), 6.23 (s, 1H), 3.55 (t, J = 5.4 Hz, 2H), 3.04 (t, J = 5.1 Hz, 2H), 2.29(s, 3H). ^{13}C NMR (75 MHz, $CDCl_3$) δ_C 189.8, 163.6, 160.4, 146.1, 142.4, 135.4, 131.1, 126.1, 124.1, 123.9, 123.1, 118.3, 38.4, 25.2, 12.0. ESI/HRMS (m/z) $[M+H]^+$ 472.0972. Calcd for $[C_{22}H_{17}FNO_4]$: 472.0984.

*4.1.1.3.5. N-(2′-(8′′-hydroxy-3′′-methyl-1′′,4′′-dioxo-1,4-dihydronaphthalen-2′′-yl)ethyl)-4-methoxybenzamide (**7e**).* Yellow oil, 109 mg (30% yield). ^{1}H NMR (300 MHz, $CDCl_3$) δ_H 12.06 (s, 1H), 7.68 (m, 2H), 7.51 (t, J = 8.1 Hz, 2H), 7.17 (t, J = 8.7 Hz, 1H), 6.84 (d, J = 7.5 Hz, 2H), 6.44 (s, 1H), 3.78(s, 3H), 3.56 (d, J = 5.7 Hz, 2H), 2.94 (t, J = 6.3 Hz, 2H), 2.19(s, 3H, CH_3). ^{13}C NMR (75 MHz, $CDCl_3$) δ_C

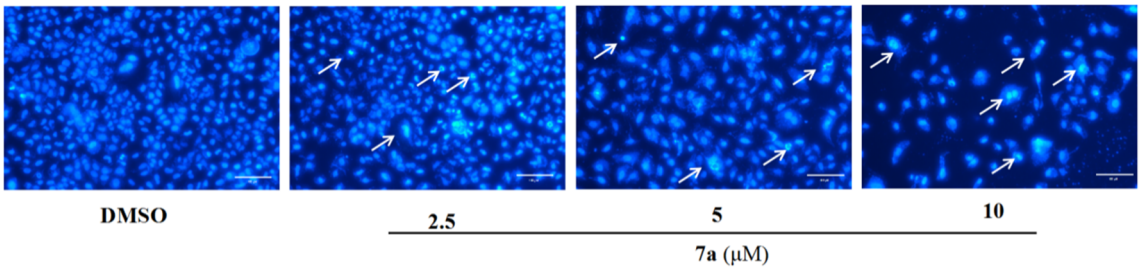

Fig. 10. The morphological apoptosis induced by **7a** in MDA-MB-321cells. MDA-MB-321 cells were treated with **7a** or DMSO for 48 h. Fluorescence microscopy images of MDA-MB-231 cells stained with Hoechst 33342.

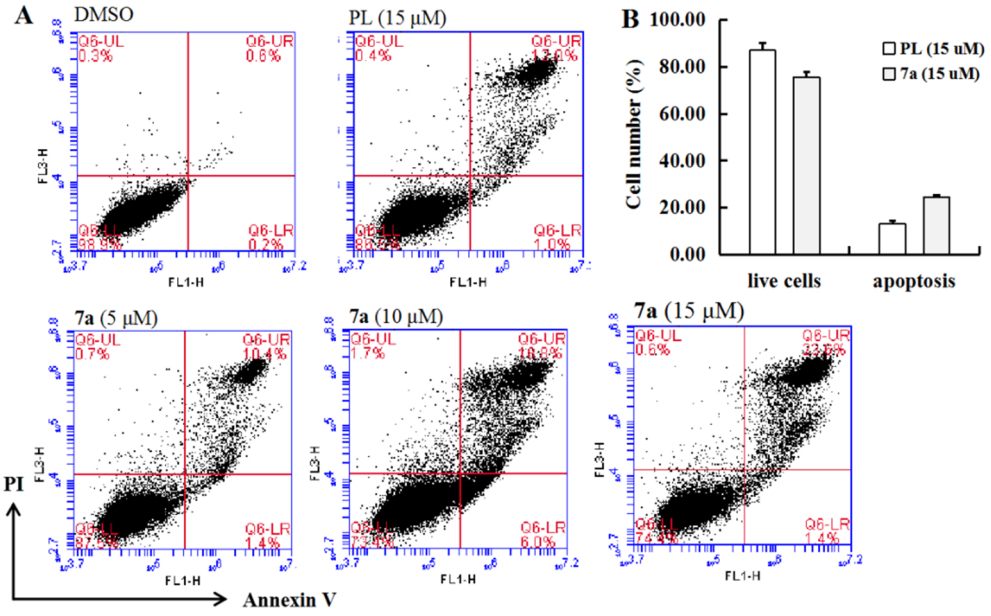

Fig. 11. Apoptotic effects of **7a** and PL in MDA-MB-231 cells. Treatment with DMSO or **7a** or PL for 48 h, MDA-MB-231 cells were collected and stained with Annexin V/PI, followed by flow cytometric analysis. (A) Flow cytometry analysis of MDA-MB-231 cells treated with DMSO, **7a** and PL. (B) Representative histograms for the numbers of living cells and apoptotic cells (%). The values were presented as the mean ± SD (n = 3).

189.5, 183.1, 166.2, 160.3, 142.7, 135.2, 128.4, 127.6, 125.4, 122.9, 118.1, 112.8, 112.7, 54.4, 38.0, 25.6, 12.1. ESI/HRMS (*m/z*) $[M+H]^+$ 366.1332. Calcd for $[C_{21}H_{20}NO_5]$: 366.1341.

*4.1.1.3.6. 4-fluoro-N-(2′-(8′′-hydroxy-3′′-methyl-1′′,4′′-dioxo-1,4-dihydronaphthalen-2′′-yl)ethyl)benzamide (**7f**).* Yellow oil, 141 mg (40% yield). ^{1}H NMR (300 MHz, $CDCl_3$) δ_H 12.10 (s, 1H), 7.75 (d, *J* = 5.4 Hz, 2H), 7.57 (m, 2H), 7.24 (t, *J* = 7.2 Hz, 1H), 7.10 (t, *J* = 6.9 Hz, 2H), 6.57 (s, 1H), 3.64 (d, *J* = 5.4 Hz, 2H), 3.01 (t, *J* = 6.0 Hz, 2H), 2.26 (s, 3H). ^{13}C NMR (75 MHz, $CDCl_3$) δ_C 190.6, 166.7, 161.3, 146.9, 143.7, 136.3, 132.1, 129.2, 129.1, 124.0, 119.2, 115.8, 115.5, 115.4, 39.1, 26.5, 13.1. ESI/HRMS (*m/z*) $[M+H]^+$ 354.1136. Calcd for $[C_{20}H_{17}FNO_4]$: 354.1142.

*4.1.1.3.7. N-(2′-(8′′-hydroxy-3′′-methyl-1′′,4′′-dioxo-1,4-dihydronaphthalen-2′′-yl)ethyl)-4-methylbenzamide (**7 g**).* Yellow oil, 147 mg (42% yield). ^{1}H NMR (300 MHz, $CDCl_3$) δ_H 12.12 (s, 1H), 7.60 (m, 4H), 7.23 (m, 3H), 6.53 (s, 1H), 3.64 (q, *J* = 6.6 Hz, 2H), 3.01 (t, *J* = 6.9 Hz, 2H), 2.39 (s, 3H), 2.26 (s, 3H). ^{13}C NMR (75 MHz, $CDCl_3$) δ_C 189.5, 183.1, 166.7, 160.2, 142.7, 141.0, 135.2, 131.1, 128.9, 128.3, 125.8, 122.9, 118.2, 38.0, 25.5, 20.4, 12.1. ESI/HRMS (*m/z*) $[M+H]^+$ 350.1388. Calcd for $[C_{21}H_{20}NO_4]$: 350.1392.

*4.1.1.3.8. N-(2-(3-methyl-1,4-dioxo-1,4-dihydronaphthalen-2-yl) ethyl)benzamide (**8a**).* Yellow oil, 143 mg (42% yield). ^{1}H NMR (300 MHz, $CDCl_3$) δ_H 7.65 (d, *J* = 8.1 Hz, 2H), 7.55 (m, 2H), 7.38 (m, 3H), 7.16 (dd, *J* = 7.8 Hz, 1.8 Hz, 2H), 6.50 (s, 1H), 3.58 (q, *J* = 6.6 Hz, 2H), 2.95 (t, *J* = 6.9 Hz, 2H), 2.20(s, 3H). ^{13}C NMR (75 MHz, $CDCl_3$) δ_C 174.2, 142.9, 132.7, 132.5, 130.5, 127.6, 125.8, 125.4, 125.3, 123.3, 38.2, 25.8, 13.1. ESI/HRMS (*m/z*) $[M+Na]^+$ 342.1095. Calcd for $[C_{120}H_{17}NNaO_3]$: 342.1106.

*4.1.1.3.9. N-(2′-(3′′-methyl-1′′,4′′-dioxo-1,4-dihydronaphthalen-2-yl) ethyl)-4-nitrobenzamide (**8b**).* Yellow oil, 157 mg (43% yield). ^{1}H NMR (300 MHz, $CDCl_3$) δ_H 8.08 (m, 2H), 7.72 (m, 4H), 7.45 (m, 2H), 6.70 (s, 1H), 3.65 (q, *J* = 6.1 Hz, 2H), 3.03 (t, *J* = 6.9 Hz, 2H), 2.28 (s, 3H). ^{13}C NMR (75 MHz, $CDCl_3$) δ_C 186.4, 184.7, 165.4, 145.8, 143.8, 140.0, 134.0, 133.7, 128.1, 126.6, 126.4, 123.9, 39.5, 26.5, 12.9. ESI/HRMS (*m/z*) $[M+H]^+$ 365.1128. Calcd for $[C_{20}H_{17}N_2O_5]$: 365.1137.

*4.1.1.3.10. 2-fluoro-N-(2′-(3′′-methyl-1′′,4′′-dioxo-1,4-dihydronaphthalen-2′′-yl)ethyl)benzamide (**8c**).* Yellow oil, 101 mg (38% yield). ^{1}H NMR (300 MHz, $CDCl_3$) δ_H 8.08 (m, 3H), 7.70 (m, 2H), 7.46 (dd, *J* = 13.2 Hz, 6.0 Hz, 1H), 7.24 (d, *J* = 7.5 Hz, 2H), 7.08 (s, 1H), 3.67 (d, *J* = 6.0 Hz, 2H), 3.04 (t, *J* = 6.9 Hz, 2H), 2.28(s, 3H). ^{13}C NMR (75 MHz, $CDCl_3$) δ_C 184.0, 184.0, 161.2, 144.3, 142.7, 132.6, 132.5, 130.9, 130.9, 125.3, 123.8, 123.8, 115.1, 114.8, 38.1, 26.0, 12.0. ESI/HRMS (*m/z*) $[M+H]^+$ 338.1189. Calcd for $[C_{20}H_{17}FNO_3]$: 338.1192.

*4.1.1.3.11. N-(2′-(3′′-methyl-1′′,4′′-dioxo-1,4-dihydronaphthalen-2′′-yl)ethyl)-3,5-bis(trifluoromethyl)Benzamide (**8d**).* Yellow oil, 150 mg (33% yield). ^{1}H NMR (300 MHz, $CDCl_3$) δ_H 8.15 (s, 2H), 8.02 (m, 2H), 7.92 (s, 1H), 7.66 (m, 2H), 7.03 (s, 1H), 3.61 (t, *J* = 5.7 Hz, 2H), 2.97 (t, *J* = 6.3 Hz, 2H), 2.24(s, 3H). ^{13}C NMR (75 MHz, $CDCl_3$) δ_C 185.6, 183.7, 163.4, 144.8, 142.6, 135.1, 133.0, 132.7, 131.0, 126.2, 125.5, 125.3, 124.0, 38.5, 25.3, 11.8. ESI/HRMS (*m/z*) $[M+H]^+$ 456.1033. Calcd for $[C_{22}H_{16}F_6NO_4]$: 456.1034.

*4.1.1.3.12. 4-methoxy-N-(2′-(3′′-methyl-1′′,4′′-dioxo-1,4-dihydronaphthalen-2′′-yl)ethyl)benzamide (**8e**).* Yellow oil, 122 mg (35% yield). ^{1}H NMR (300 MHz, $CDCl_3$) δ_H 8.01 (m, 2H), 7.65 (m, 4H), 6.85 (t, *J* = 6.9 Hz, 2H), 6.53 (s, 1H), 3.77 (s, 3H), 3.55 (q, *J* = 6.6 Hz, 2H), 2.94 (t, *J* = 6.9 Hz, 2H), 2.21 (s, 3H). ^{13}C NMR (75 MHz, $CDCl_3$) δ_C 184.7, 183.9, 166.1, 144.5, 143.0, 132.6, 131.0, 130.9, 127.6, 125.4, 125.3, 123.4, 118.0, 112.7, 54.4, 38.1, 25.9, 11.9. ESI/HRMS (*m/z*) $[M+H]^+$ 350.1388. Calcd for $[C_{21}H_{20}NO_4]$: 350.1392.

*4.1.1.3.13. 4-fluoro-N-(2′-(3′′-methyl-1′′,4′′-dioxo-1,4-dihydronaphthalen-2′′-yl)ethyl)benzamide (**8f**).* Yellow oil, 128 mg (38% yield). ^{1}H NMR (300 MHz, $CDCl_3$) δ_H 8.02 (m, 2H), 7.66 (m, 4H), 7.02 (t, *J* = 8.4 Hz, 2H), 6.64 (s, 1H), 3.56 (q, *J* = 6.6 Hz, 2H), 2.94 (t, *J* = 6.6 Hz, 2H), 2.20(s, 3H), 2.26(s, 3H). ^{13}C NMR (75 MHz, $CDCl_3$) δ_C 185.9, 184.8, 166.5, 145.6, 143.9, 133.8, 133.6, 129.3, 129.1, 126.4, 126.3, 115.7, 115.4, 39.2, 26.8, 12.9. ESI/HRMS (*m/z*) $[M+H]^+$ 338.1189. Calcd for $[C_{20}H_{17}FNO_3]$: 338.1192.

*4.1.1.3.14. 4-methyl-N-(2′-(3′′-methyl-1′′,4′′-dioxo-1,4-dihydronaphthalen-2′′-yl)ethyl)benzamide (**8g**).* Yellow oil, 133 mg (40% yield). ^{1}H NMR (300 MHz, $CDCl_3$) δ_H 8.01 (m, 2H), 7.59 (m, 4H), 7.14 (d, *J* = 8.4 Hz, 2H), 6.59 (s, 1H), 3.56 (q, *J* = 6.6 Hz, 2H), 2.94 (t, *J* = 6.6 Hz, 2H), 2.31(s, 3H), 2.20(s, 3H). ^{13}C NMR (75 MHz, $CDCl_3$) δ_C 184.6, 183.9, 166.7, 144.5, 142.9, 132.6, 131.1, 131.0, 128.2, 128.1, 125.8, 125.3, 125.2, 38.1, 25.9, 20.4, 11.9. ESI/HRMS (*m/z*) $[M+H]^+$ 334.1430. Calcd for $[C_{21}H_{20}NO_3]$: 334.1443.

*4.1.1.3.15. N-(2′-(8′′-hydroxy-3′′-methyl-1′′,4′′-dioxo-1,4-dihydronaphthalen-2′′-yl)ethyl)isonicotinamide (**9a**).* Yellow oil, 151 mg (45% yield). ^{1}H NMR (300 MHz, $CDCl_3$) δ_H 12.07 (s, 1H), 8.75 (dd, *J* = 4.5 Hz, 1.5 Hz, 2H), 7.51 (m, 4H), 7.16 (dd, *J* = 7.5 Hz, 2.1 Hz, 2H), 6.68 (d, *J* = 5.1 Hz, 1H), 3.59 (q, *J* = 6.9 Hz, 2H), 2.95 (t, *J* = 6.9 Hz, 2H), 2.19(s, 3H). ^{13}C NMR (75 MHz, $CDCl_3$) δ_C 185.1, 178.7, 162.2, 155.9, 150.7, 138.3, 130.8, 123.9, 121.3, 118.5, 113.8, 109.4, 33.6, 21.1, 13.0. ESI/HRMS (*m/z*) $[M+H]^+$ 337.1178. Calcd for $[C_{19}H_{17}N_2O_4]$: 337.1188.

*4.1.1.3.16. N-(2′-(3′′-methyl-1′′,4′′-dioxo-1,4-dihydronaphthalen-2′′-yl)ethyl)isonicotinamide (**9b**)*. Yellow oil, 134 mg(42% yield). ^{1}H NMR (300 MHz, $CDCl_3$) δ_H 8.67 (dd, J = 4.5 Hz, 1.8 Hz, 2H), 7.50 (m, 4H), 7.16 (dd, J = 7.5 Hz, 2.1 Hz, 2H), 6.68 (d, J = 5.7 Hz, 1H), 3.59 (q, J = 6.6 Hz, 2H), 2.95 (t, J = 6.9 Hz, 2H), 2.19(s, 3H). ^{13}C NMR (75 MHz, $CDCl_3$) δ_C 180.1, 179.3, 158.1, 152.1, 139.9, 127.9, 123.7, 120.7, 33.5, 21.4, 15.9. ESI/HRMS (m/z) $[M+H]^+$ 321.1189. Calcd for $[C_{19}H_{17}N_2O_3]$: 321.1239.

*4.1.1.4. Syntheses of **11***. Succinic acids (495 mg, 4.5 mmol, 3.0 eq), $AgNO_3$ (76 mg, 0.45 mmol, 0.3 eq) were successively added to a solution of PL (282 mg, 1.5 mmol, 1.0 eq) in 30% aqueous acetonitrile (20 mL) at 60 ˚C. when reaction system heated to 70 ˚C, a solution of ammonium persulfate (444.6 mg, 1.95 mmol, 1.3 eq) in 30% aqueous acetonitrile (12 mL) was added dropwise over 30 min, and the resulting solution stirred at 65–70 ˚C for 3–4 h. On cooling, the mixture was extracted with EtOAc (3 × 30 mL), and the organic layer washed with H_2O (3 × 30 mL), dried (Na_2SO_4) and solvent evaporated. The crude material was purified via column chromatography (CH_2Cl_2/MeOH = 20:1) to yield the intermediate **10** (247 mg, 61%). PyBop (310 mg, 0.55 mmol), DMAP (72.5 mg, 0.55 mmol), TEA (101 mg, 1 mmol) were successively added to a solution of intermediate **10** (135 mg, 0.5 mmol) in dry CH_2Cl_2 (10 mL). A solution of aniline (116 mg, 1.3 mmol) in dry CH_2Cl_2 (2 mL). was added slowly and the resulting solution stirred at room temperature for 24 h. The completion of reaction was monitored by TLC. After completion, poured into 10 mL of CH_2Cl_2, washed with 5% HCl (20 mL × 3) and saturated NaCl (20 mL × 2), dried (Na_2SO_4) and solvent evaporated. The crude material was purified via column chromatography (CH_2Cl_2/MeOH = 100:1) to yield the orange powder (50 mg, 30%).

*4.1.1.4.1. 3′-(8′′-hydroxy-3′′-methyl-1′′,4′′-dioxo-1,4-dihydronaphthalen-2′′-yl)-N-phenylpropanamide (**11**)*. Orange powder, 50 mg (30% yield). M.p.102–104 ˚C. ^{1}H NMR (300 MHz, $CDCl_3$): δ_H 12.12 (s, 1H), 7.60 (m, 2H), 7.50 (d, J = 6.0 Hz, 2H), 7.32 (t, J = 7.5 Hz, 3H), 7.22 (dd, J = 7.8 Hz, 1.5 Hz, 1H), 7.11 (t, J = 7.5 Hz, 1H), 3.07 (t, J = 7.8 Hz, 2H), 2.60 (t, J = 7.5 Hz, 2H), 2.26(s, 3H). ^{13}C NMR (75 MHz, $CDCl_3$) δ_C 190.5, 161.3, 146.9, 143.7, 136.2, 131.6, 128.6, 126.8, 123.9, 119.2, 33.0, 20.5, 13.1. ESI/HRMS (m/z) $[M+H]^+$ 336.1227. Calcd for $[C_{20}H_{17}NO_4]$: 336.1236.

*4.1.1.5. Syntheses of **12***. $Cu(AcO)_2$ (9.9 mg, 0.05 mmol), aniline (46.5 mg, 0.5 mmol) were successively added to a solution of PL (94 mg, 0.5 mmol) in glacial acetic acid (2 mL), and the mixture was stirred at 60 ˚C for 4 h. Diluted with water (20 mL), extracted with EtOAc (3 × 15 mL), and the organic layer washed with H_2O (3 × 15 mL) and saturated NaCl (15 mL × 1), dried (Na_2SO_4) and solvent evaporated. The crude material was purified via column chromatography (PE/EA = 2:1, v / v) to yield the purple solid **12** (44 mg, 32%).

*4.1.1.5.1. 5-hydroxy-2-methyl-3-(phenylamino)naphthalene-1,4-dione (**12**)*. Orange powder, 44 mg (34% yield). M.p.113–116 ˚C. ^{1}H NMR (300 MHz, $CDCl_3$) δ_H 11.60 (s, 1H), 7.65 (m, 2H), 7.34 (t, J = 8.4 Hz, 3H), 7.18 (dd, J = 7.8 Hz, 1.5 Hz, 1H), 7.13 (t, J = 7.2 Hz, 1H), 6.97 (d, J = 7.5 Hz, 2H), 1.73(s, 3H). ^{13}C NMR (75 MHz, $CDCl_3$) δ_C 189.5, 166.2, 145.8, 142.7, 135.2, 130.6, 127.6, 125.8, 125.8, 122.9, 118.2, 12.1. ESI/HRMS (m/z) $[M+H]^+$ 280.0963. Calcd for $[C_{17}H_{14}NO_3]$: 280.0974.

*4.1.1.6. Syntheses of **13***. Dissolved PL (94 mg, 0.5 mmol) in MeOH (5 mL) under N_2. NaN_3 (3.5 mmol) was dissolved in water (2 mL) and acidified to pH 4. To a solution of PL was added NaN_3 solution and slowly heated reaction to 50 ˚C and stirred for 5 h. Reaction was quenched with water and extracted with ethyl acetate (10 mL × 3). The organic layers were combined and washed with saturated NaCl solution, dried over anhydrous Na_2SO_4, and concentrated in vacuum. The reaction was purified on silica gel eluting with PE/EA (10:1 to 5:1) to yield the purple solid **13** (37 mg, 37%).

*4.1.1.6.1. 3-amino-5-hydroxy-2-methyl-1,4-naphthoquinone (**13**)*. Orange powder, 37 mg (37% yield). M.p.108–110 ˚C. ^{1}H NMR (300 MHz, DMSO-d_6) δ_H 11.55 (1H, s), 7.76 (1H, d, J = 7.8 Hz), 7.48 (1H, d, J = 8.1 Hz), 7.24 (1H, d, J = 8.4 Hz), 5.84 (2H, brs), 2.01 (3H, s). ^{13}C NMR (75 MHz, DMSO-d_6) δ_C 186.6, 181.5, 160.7, 150.7, 137.8, 133.9, 122.2, 117.9, 114.6, 103.0, 12.0; HREIMS m/z 204.0655 $[M+H]^+$ (calcd for $C_{11}H_{10}NO_3$, 204.0655).

4.2. Biological Experiments.

4.2.1. Cytotoxic assay in vitro

The antiproliferative activities of test compounds were investigated by the MTT method. Briefly, human cancer cell lines such as MDA-MB-231, A549 and HepG2 cells, or normal human cell line PBMCs and HFL-1 cells at a final density of 5.0 × 10^4/ml were seeded into 96-well plates and allowed to adhere for 24 h. After treated with or without different concentrations of test compounds for 48 h, the cells were exposed to MTT (5 mg/mL), and the plate was further incubated in 37 ˚C CO_2 incubator for another 4 h. Abandoned supernatant before adding 100 μL DMSO to each well. Optical density (OD) was measured using spectrophotometer at 570 nm. The number of viable cells was determined from the absorbance. Assays were performed in triplicate wells. Data are presented as the mean ± SD (n = 3).

4.2.2. Molecular Modeling.

The X-ray structure of the STAT3 (1BG1) was used. The molecular docking software used in this study was Autodock Vina 1.1.2. The parameters were set to “center x = 101.9; center y = 83.0; center z = 66.2; size x = 20; size y = 20; size z = 0”.

4.2.3. Western blot analysis

Cells were seeded in 10 cm plates and allowed to adhere overnight. The cells were serum-starved. The cells were then treated with DMSO or **7a**. After 6 h, cells were stimulated by IL-6 (25 ng/mL) or IFN (25 ng/mL). The cells were harvested after 30 min and analyzed by Western blot.

4.2.4. Hoechst-33342 Staining.

MDA-MB-231 cells (4 × 10^5 cells) were incubated in 6 cm dish for 24 h. Then the cells were treated with the DMSO/**7a** at indicated concentrations for 24 h. Cells were washed twice by PBS. Then cells were incubated with Hoechst-33342 (10 μg/ml) for 5 min at room temperature in the darkness. After incubation, stained cells were observed under a fluorescent microscope (CORPORATION, Japan).

4.2.5. Cell apoptosis analysis

MDA-MB-231 cells (4 × 10^5 cells) were incubated in 6 cm dish for 48 h. Then DMSO/**7a**/PL was added to the cells with indicated concentrations. After another incubation of 48 h, the cells were harvested softly and washed twice with cold PBS (2000 *g* for 5 min). Then the cells were added to 250 μL binding buffer containing 2.5 μL PI and 2.5 μL Annexin V (KeyGEN, China). The mixture was incubated at room temperature for 15 min in the darkness and analyzed by flow cytometry.

Declaration of Competing Interest

The authors declare that they have no known competing financial interests or personal relationships that could have appeared to influence the work reported in this paper.

Acknowledgements

This research has been supported by the Academic Innovation

Project of Jiangsu Department of Education (No. 1150021667) and "Double First Class" Subject Innovation Team Construction Project of China Pharmaceutical University (CPU2018GY12).

Appendix A. Supplementary data

Supplementary data to this article can be found online at https://doi.org/10.1016/j.bioorg.2020.104208.

References

[1] J. Bromberg, J.E. Darnell, The role of STATs in transcriptional control and their impact on cellular function, Oncogene. 19 (2000) 2468–2473.

[2] T. Hirano, K. Ishihara, M. Hibi, Roles of STAT3 in mediating the cell growth, differentiation and survival signals relayed through the IL-6 family of cytokine receptors, Oncogene. 19 (2000) 2548–2556.

[3] S. Haftchenary, M. Avadisian, P.T. Gunning, Inhibiting aberrant Stat3 function with molecular therapeutics: a progress report, Anticancer Drugs. 22 (2011) 115–127.

[4] B.D.G. Page, D.P. Ball, P.T. Signal transducer and activator of transcription 3 inhibitors: a patent review. Expert Opin. Ther. Pat. 21 (2011) 65–83.

[5] S. Fletcher, J. Turkson, P.T. Molecular approaches towards the inhibition of the signal transducer and activator of transcription 3 (Stat3) protein. Gunning. Chem. Med. Chem. 3 (2008) 1159–1168.

[6] W. Yu, H. Xiao, J. Lin, C. Li, Discovery of novel STAT3 small molecule inhibitors via in silico site-directed fragment-based drug design, J. Med. Chem. 56 (2013) 4402–4412.

[7] P.K. Mandal, F. Gao, Z. Lu, Potent and selective phosphopeptide mimetic prodrugs targeted to the Src homology 2 (SH2) domain of signal transducer and activator of transcription 3, J. Med. Chem. 54 (2011) 3549–3563.

[8] L.B. Mora, R. Buettner, J. Seigne, J. Diaz, N. Ahmad, R. Garcia, T. Bowman, R. Falcone, R. Fairclough, A. Cantor, C. Muro-Cacho, S. Livingston, J. Karras, J. Pow-Sang, R. Constitutive activation of Stat3 in human prostate tumors and cell lines: direct inhibition of Stat3 signaling induces apoptosis of prostate cancer cells. Jove. Cancer Res. 62 (2002) 6659–6666.

[9] B.E. Barton, J.G. Karras, T.F. Murphy, A. Barton, H.F. Huang, Signal transducer and activator of transcription 3 (STAT3) activation in prostate cancer: Direct STAT3 inhibition induces apoptosis in prostate cancer lines, Mol. Cancer Ther. 3 (2004) 11–20.

[10] S. Fletcher, J.A. Drewry, V.M. Shahani, B.D. Page, P.T. Gunning, Molecular disruption of oncogenic signal transducer and activator of transcription 3 (STAT3) protein, Biochem. Cell Biol. 87 (2009) 825–833.

[11] B.D. Page, D.C. Croucher, Z.H. Li, S. Haftchenary, V.H. Jimenez-Zepeda, J. Atkinson, P.A. Spaqnuolo, Y.L. Wong, R. Colaquori, A.M. Lewis, A.D. Schimmer, S. Truder, P.T. Gunning, Inhibiting aberrant signal transducer and activator of transcription protein activation with tetrapodal, small molecule src homology 2 domain binders: promising agents against multiple myeloma, J. Med. Chem. 56 (2013) 7190–7200.

[12] S. Fletcher, B.D. Page, X. Zhang, P. Yue, Z.H. Li, S. Sharmeen, J. Singh, W. Zhao, A.D. Schimmer, S. Truder, J. Turkson, P.T. Gunning, Antagonism of the Stat3–Stat3 protein dimer with salicylic acid based small molecules, Chem. Med. Chem. 6 (2011) 1459–1470.

[13] H. Yu, R. Jove, The STATs of cancer-new molecular targets come of age, Nat. Rev. Cancer. 4 (2004) 97–105.

[14] O.S. Lee, W. Lou, K.M. Qureshi, F. Mehraein-Ghomi, D.L. Trump, A.C. Gao, RNA interference targeting Stat3 inhibits growth and induces apoptosis of human prostate cancer cells, Prostate. 60 (2004) 303–309.

[15] L. Gao, L. Zhang, J. Hu, F. Li, Y. Shao, D. Zhao, D.V. Kalvakolanu, D.J. Kopecko, X. Zhao, D.Q. Xu, Down-regulation of signal transducer and activator of transcription 3 expression using vector-based small interfering rnas suppresses growth of human prostate tumor in vivo, Clin Cancer Res. 11 (2005) 6333–6341.

[16] H. Song, R. Wang, S. Wang, J. Lin, A low-molecular-weight compound discovered through virtual database screening inhibits Stat3 function in breast cancer cells, Proc. Natl. Acad. Sci. U.S.A. 102 (2005) 4700–4705.

[17] L. Lin, D.M. Benson Jr., S. Deangelis, C.E. Bakan, P.K. Li, C. Li, J. Lin, A small molecule, LLL12 inhibits constitutive STAT3 and IL-6-induced STAT3 signaling and exhibits potent growth suppressive activity in human multiple myeloma cells, Int. J. Cancer. 130 (2012) 1459–1469.

[18] L. Lin, B. Hutzen, P.K. Li, S. Ball, M. Zuo, S. DeAngelis, E. Foust, M. Sobo, L. Friedman, D. Bhasin, L. Cen, C. Li, J. Lin, A novel small molecule, LLL12, inhibits STAT3 phosphorylation and activities and exhibits potent growth-suppressive activity in human cancer cells, Neoplasia 12 (2010) 39–50.

[19] S. Ball, C. Li, P.K. Li, J. Lin, The small molecule, LLL12, inhibits STAT3 phosphorylation and induces apoptosis in medulloblastoma and glioblastoma cells, PLoS One. 6 (2011) e18820.

[20] D. Bhasin, K. Cisek, T. Pandharkar, N. Regan, C. Li, B. Pandit, J. Lin, P.K. Li, Design, synthesis, and studies of small molecule STAT3 inhibitors, Bioorg Med Chem Letters. 18 (2008) 391–395.

[21] J. Turkson, D. Ryan, J.S. Kim, Y. Zhang, Z. Chen, E. Haura, A. Laudano, S. Sebti, A.D. Hamilton, R. Jove, Phosphotyrosyl peptides block Stat3-mediated DNA binding activity, gene regulation, and cell transformation, J Biol Chem. 276 (2001) 45443–45455.

[22] J. Turkson, J.S. Kim, S. Zhang, J. Yuan, M. Huang, M. Glenn, E. Haura, S. Sebti, A.D. Hamilton, R. Jove, Novel peptidomimetic inhibitors of signal transducer and activator of transcription 3 dimerization and biological activity, Mol Cancer Ther. 3 (2004) 261–269.

[23] Chinese Herbalism Editorial Board, State Administration of Traditional Chinese Medicine of the People's Republic of China. Zhong Hua Ben Cao, 6, Shanghai Science and Technology Press, (2000) 132.

[24] A.A. Aly, E.M. El-Sheref, M.E.M. Bakheet, M.A.E. Mourad, A.B. Brown, S. Bräse, M. Nieger, M.A.A. Ibrahim, Synthesis of novel 1,2-bis-quinolinyl-1,4-naphthoquinones: ERK2 inhibition, cytotoxicity and molecular docking studies, Bioorganic Chem. 81 (2018) 700–712.

[25] A.A. Aly, E.M. El-Sheref, M.E.M. Bakheet, M.A.E. Mourad, S. Bräse, M.A.A. Ibrahim, M. Nieger, B.K. Garvalov, K.N. Dalby, T.S. Kaoud, Design, synthesis and biological evaluation of fused naphthofuro[3,2-c] quinoline-6,7,12-triones and pyrano[3,2-c] quinoline-6,7,8,13-tetraones derivatives as ERK inhibitors with efficacy in BRAF-mutant melanoma, Bioorganic Chem. 82 (2019) 290–305.

[26] W. Yan, B. Tu, Y.Y. Liu, T.Y. Wang, H. Qiao, Z.J. Zhai, H.W. Li, T.T. Tang, Suppressive effects of plumbagin on invasion and migration of breast cancer cells via the inhibition of STAT3 signaling and down-regulation of inflammatory cytokine expressions, Bone Res. 1 (2013) 362–370.

[27] O. Trott, A.J. Olson, AutoDock Vina: improving the speed and accuracy of docking with a new scoring function, efficient optimization and multithreading, J. Comput. Chem. 31 (2010) 455–461.

[28] G. Naturale, M. Lamblin, C. Commandeur, F.X. Felpin, J. Dessolin, Direct C-H alkylation of naphthoquinones with amino acids through a revisited Kochi-Anderson radical decarboxylation: trends in reactivity and applications, Eur. J. Org. Chem. 44 (2013) 5774–5788.

[29] Y. Zhang, Z.Y. Liu, STAT1 in cancer: friend or foe? Discov. Med. 24 (2017) 19–29.